Chapter 11

Indirect Off-Axis Holography for Antenna Metrology

Ana Arboleya, Jaime Laviada, Juha Ala-Laurinaho,

Yuri Álvarez, Fernando Las-Heras and

Antti V. Räisänen

Additional information is available at the end of the chapter

http://dx.doi.org/10.5772/67294

Abstract

Phase acquisition in antenna measurement, especially at millimeter- and submillimeter-wave frequencies, is an expensive and challenging task. The need of a steady phase reference demands not only a very stable source but unvarying temperature conditions and strong positioning accuracy requirements. Indirect off-axis holography is an interferometric technique that allows for characterization of an unknown field by means of a simple filtering process of the hologram or intensity interference pattern in the spectral domain, provided that the reference field, employed to interfere with the unknown field, is known in amplitude and phase. This technique can be used to avoid the effect of the errors related to the phase acquisition and to further develop new efficient and robust techniques capable of phase retrieval from amplitude-only acquisitions allowing for cost and complexity reduction of the measurement setup. A short review of the state-of-the-art in antenna metrology is presented in this chapter, as well as a description of conventional indirect off-axis techniques applied to this field. Last sections are devoted to the description of novel measurement techniques developed by the authors in order to overcome the main limitations of the conventional methods.

Keywords: antenna measurement, antenna diagnostics, amplitude-only, interferometry, off-axis holography, indirect holography, phaseless, microwave holography, millimeter-wave, submillimeter-wave

1. Introduction

Antenna measurement techniques are devoted to obtaining the main radiation parameters (radiation pattern, antenna gain, polarization, etc.) in the antenna far-field (FF) region[1] from the acquisition of the fields radiated by the antenna under test (AUT). Novel methods for antenna measurement [1] and postprocessing techniques [2] are constantly emerging to cope with the requirements needed to provide efficient and accurate characterization of new types of antennas, mainly at high frequency bands. Additionally, antenna diagnostics enables nondestructive inspection of the antennas for detection of design or fabrication failures by means of the analysis of their extremely near fields or their equivalent currents [3–6].

First, antenna measurements were performed in outdoor ranges at FF distances. Those tests were highly affected by weather conditions, interference, and multipath from multiple reflections mainly caused by the floor. Anechoic chamber testing was sooner adopted as the standard method for antenna metrology. Anechoic chambers have an electromagnetic absorber lining to reduce electromagnetic reflections and to control the measurement environment [7].

Advances in fabrication technologies have contributed to the development of new components and antennas at millimeter (mm-) and submillimeter (submm-) wave frequency bands.[2] At these frequencies, measurement of directive antennas would require extremely large anechoic chambers to fulfill the FF condition. Hence, other types of measurement ranges such as near-field (NF) measurement ranges have been developed to avoid the previous shortcoming [1].

In NF measurement systems, the field is acquired over a surface in the vicinity of the AUT. Planar, cylindrical, or spherical surfaces are the most common acquisition surfaces, with recent extensions to arbitrary geometry [9] or noncanonical domains [10, 11]. The acquired NF can be employed to obtain the FF radiation pattern of the antenna by means of mathematical NF-FF transformations based either in wave expansions [1, 12, 13] or integral equation methods such as the sources reconstruction method (SRM) [3, 9]. Diagnostics applications can also be developed from NF data using backpropagation techniques toward the AUT aperture [1, 13] or the SRM [3, 9]. After several decades of research and development, NF ranges have become the preferred approach for antenna testing.

Special attention must be given to the probe pattern and positioning accuracy [1] as well as to the effects that error sources in NF acquisitions, such as truncation of the measurement plane, cable flexing, stray signals, leakage, etc., can introduce in the FF pattern of the AUT [1, 2, 13, 14].

---

[1]The far-field distance is defined by $R = 2D^2/\lambda$ ($R >> \lambda$), being D the maximum dimension of the antenna and λ the wavelength [1].

[2]The mm-wave band is defined according to the IEEE Standard 521-2002 from 110 to 300 GHz. This standard is a review of the standard published in 1984 that also considered the lower bands defined from 30 to 110 GHz (Ka, V, and W bands) as part of the mm-wave band. This older definition is still commonly accepted. Frequency bands above 300 GHz are not included in the standard; the submm-wave or Terahertz band corresponds, depending on the author, to the fraction of the spectrum from 300 GHz to either 3 or 10 THz in the lower limit of the far-infrared spectrum [8].

NF techniques for both NF-FF transformation and antenna diagnostics generally require the knowledge of amplitude and phase of the radiated electric field by the AUT [1–5]. Nevertheless, phase acquisition, particularly at mm- and submm-wave bands, is a challenging task that requires sophisticated and expensive equipment due to the high thermal stability requirements and the effect of the errors, mostly resulting from thermal drift and cable flexing [1, 13–16].

Nowadays research is focused on the development of new measurement systems [17, 18] and techniques that allow reducing the acquisition time and costs and preventing or correcting the effect of errors in NF measurements [2–7, 19]. Among these techniques, amplitude-only measurements, commonly referred to as phaseless or scalar measurements (in contrast to vector, also referred to as complex measurements involving amplitude and phase), are frequently employed due to their multiple advantages such as the use of simpler and less expensive receivers and robustness to errors related to phase acquisition. Amplitude-only techniques can be indistinctly applied to antenna measurements and diagnostics and are divided into two main groups depending on the implementation approach: iterative and noniterative techniques.

On the one hand, most of the iterative techniques [3, 19, 10] are based on the acquisition of the field intensity in two or more surfaces. Then, an iterative process is employed to propagate the field from one surface to another after guessing an initial phase, until certain condition is satisfied for all the surfaces. This kind of technique is popular because they involve minor changes in the measurement setup, nevertheless they can suffer from stagnation and their convergence is strongly related to the first guess solution. On the other hand, and belonging to noniterative techniques, most of the interferometric approaches [5, 20–23] rely on the use of a reference field, previously known in amplitude and phase, used to interfere the field of the AUT and allowing an easy and iteration-free phase retrieval by means of a filtering process in the spectral domain.

Indirect off-axis holography, also known as Leith-Upatnieks holography [24], is an interferometric technique adapted from optical holography to amplitude-only antenna metrology in the early 1970s [25, 26]. During the last years, great efforts have been made to improve aspects such as sampling [22] and overlapping reduction [27] or reference signal calibration [28, 29]. The rest of the chapter is divided as follows: Section 2 contains an introduction to conventional off-axis holography techniques applied to antenna metrology. Novel techniques that allow for the use of synthesized reference waves with mechanical phase shifts [5, 30] will be introduced in Section 3. A new efficient method for amplitude-only characterization of broadband antennas [23] compatible with nonredundant sampling techniques [31] will be described in Section 4. Finally, main conclusions regarding the advantages and disadvantages of the proposed methods will be drawn in Section 5. Numerical validation of the proposed techniques in Sections 3 and 4, performed in Planar NF (PNF) measurement ranges [32, 33], will be given for each method and, thus, although easily translatable to other geometries, formulation will be particularized for planar acquisition systems.

2. Conventional indirect off-axis holography review

The word holography comes from the Greek words hólos (whole) and gráphō (written or represented) and was first coined by Gabor in 1948 to define a new technique in the optics

field for retrieving the amplitude and phase of an unknown field after recording the intensity of a coherent wave disturbance [34] with a reference field, whose amplitude and phase could be properly characterized. The technique was later adapted by Leith and Upatnieks to use an off-axis reference [24].

The term holography has been subsequently employed in the context of antenna metrology and electromagnetic imaging to refer to another technique in which the phase information is directly acquired with the amplitude and a cable reference is employed (direct holography) [35, 36]. Thus, to avoid confusion, the methods described in this chapter will be referred to as *indirect off-axis holography,* since the phase is indirectly measured.

2.1. Indirect off-axis holography

Indirect off-axis techniques are based on two-step procedures: (1) recording the intensity of the interference pattern formed by the AUT and the reference field and (2) performing the phase retrieval of the unknown field (AUT's field) by means of a filtering process of the recorded pattern or hologram in the spectral domain. Conventional setup is usually implemented as shown in **Figure 1** employing a radiated reference field [21, 25] that is obtained from a sample of the source by means of a directional coupler. A variable attenuator (or amplifier) is usually included in the AUT or reference branches in order to balance the power between both branches and to increase the dynamic range of the hologram.

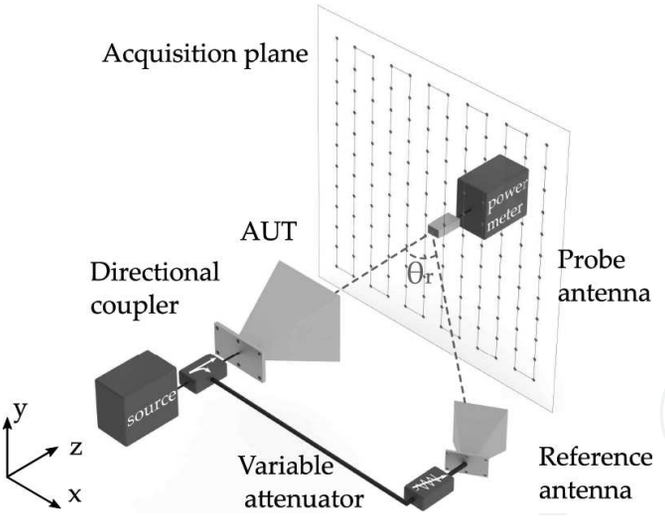

Figure 1. Basic setup for conventional indirect off-axis holography antenna measurement.

Another option is to create a plane reference wave by means of a shaped plane mirror which is employed as the collimator in compact antenna ranges [37]. Nevertheless, correctly shaping the mirror for high frequency indirect holography requires accurate and expensive machining.

The hologram is recorded at each point of the acquisition plane as the squared sum of the fields of the AUT E_{aut} and the reference antenna E_{ref} as:

http://dx.doi.org/10.5772/67294

$$H(\vec{r}) = |E_{\text{aut}}(\vec{r}) + E_{\text{ref}}(\vec{r})|^2. \tag{1}$$

The expression of the hologram can be further developed into

$$H(\vec{r}) = |E_{\text{aut}}(\vec{r})|^2 + |E_{\text{ref}}(\vec{r})|^2 + E_{\text{aut}}(\vec{r})E^*_{\text{ref}}(\vec{r}) + E^*_{\text{aut}}(\vec{r})E_{\text{ref}}(\vec{r}), \tag{2}$$

where the asterisk is used to denote complex conjugate.

If the expression in Eq. (2) is Fourier-transformed to the spatial frequency domain or k-space, the spectrum of the hologram can be expressed as

$$h(\vec{k}) = |e_{\text{aut}}(\vec{k})|^2 + |e_{\text{ref}}(\vec{k})|^2 + e_{\text{aut}}(\vec{k}) \otimes e^*_{\text{ref}}(-\vec{k}) + e^*_{\text{aut}}(-\vec{k}) \otimes e_{\text{ref}}(\vec{k}), \tag{3}$$

being e_{aut} and e_{ref} the Fourier transform (FT) of E_{aut} and E_{ref}, respectively, and $\otimes$ is the convolution operator.

As it is depicted in **Figure 2**, the spectrum of the hologram is composed of four different terms: the two zero-frequency harmonics in the center, known as autocorrelation terms, and the cross-correlation or image terms, which contain shifted and distorted (in case of using a nonplanar wave reference field) information about the complex field of the AUT.

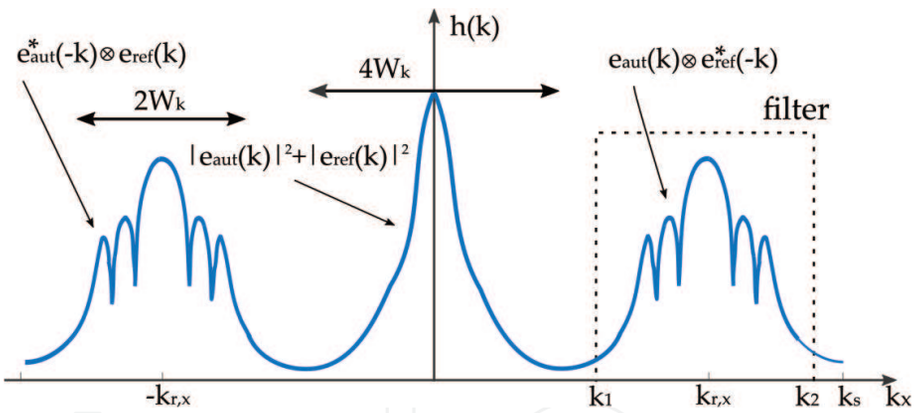

Figure 2. Schematic representation of the spectrum of the hologram for an off-axis angle in the x-axis.

Providing no overlap between the autocorrelation terms and the image term corresponding to $e_{\text{aut}}(\vec{k}) \otimes e^*_{\text{ref}}(-\vec{k})$ exists, the latter can be bandpass-filtered as

$$h_{\text{filtered}}(\vec{k}) = \Pi(\vec{k}_1, \vec{k}_2)\{e_{\text{aut}}(\vec{k}) \otimes e^*_{\text{ref}}(-\vec{k})\}, \tag{4}$$

where $\Pi(\vec{k}_1, \vec{k}_2)$ is a rectangular window defined by its corners at the spectral points $\vec{k}_1$ and $\vec{k}_2$ to filter the desired image term.

From the filtered term, the unknown field of the AUT can be easily retrieved back in the spatial domain by removing the effect of the complex conjugate of the reference field as

$$E_{\text{aut,retrieved}}(\vec{r}) = \frac{FT^{-1}\{h_{\text{filtered}}(\vec{k})\}}{E^{*}_{\text{ref}}(\vec{r})}. \tag{5}$$

It is relevant to remark that $E^{*}_{\text{ref}}(\vec{r})$ is a term whose amplitude usually suffers small changes along the spatial domain and, consequently, Eq. (5) can be evaluated without the risk of divisions by zero.

Quality of the phase retrieval will mostly depend on the degree of overlapping between the autocorrelation and cross-correlation terms, which for radiated reference fields is related to the off-axis position of the reference antenna, as it will be addressed next.

At this point it is worth noting two facts: first, the retrieved field corresponds to one of the tangential components of the electric field. In order to obtain the FF pattern of the AUT, both tangential fields are needed [1] and, thus, the process has to be repeated after turning the AUT 90° to acquire the other component [23]. Second, for the sake of simplicity, the offset of the reference antenna has only been introduced in the x-axis (as shown in **Figure 1**) without loss of generality.

2.1.1. Overlapping control: off-axis reference and sampling requirements

Central position of the image terms is defined by the off-axis angle of the reference antenna as

$$k_{r,x} = \pm k_0 \sin(\theta_r) \tag{6}$$

being k_0 the propagation vector in vacuum, defined as $k_0 = 2\pi/\lambda$, with λ the wavelength of the fields, and θ_r the off-axis angle formed by the reference antenna and the normal to the acquisition plane (see **Figure 1**).

According to Ref. [1], the maximum spatial bandwidth[3] of a radiated field in a planar acquisition is $W_k = k_0$. On the other hand, since the autocorrelation terms are the FT of a squared field, their bandwidth doubles the bandwidth of the original field [21, 28, 38] and, thus, the no overlapping condition is given by

$$k_{r,x} \geq 3k_0. \tag{7}$$

Nevertheless, due to the limitations imposed by the topology of the setup, the maximum off-axis angle is limited to 90°, yielding a maximum value of $k_{r,x\max} = k_0$. Therefore, although overlapping can be reduced by employing certain techniques (e.g., filtering after backpropagation of the planar wave spectrum (PWS) of the hologram toward the aperture or employing the so-called modified hologram, described later), it cannot be completely avoided in these setups with radiated reference waves.

[3]Bandwidth is defined for the positive half-space of the spectrum. Since the spectrum of the hologram is symmetric, the total bandwidth is twice the defined bandwidth.

On the other hand, sampling in the spatial domain is related to the extension of the *k*-space and has to be carefully selected in order to avoid aliasing. According to the *Nyquist* theorem, the extension of the *k*-space is related to the sampling step Δx by Ref. [12]:

$$k_s = \frac{\pi}{\Delta x} \tag{8}$$

As previously mentioned, the image terms are centered in k_0 ($k_{r,x} = k_{r,x\max}$) and have a bandwidth of $W_k = k_0$, yielding a total extension of $k_s = 2k_0$. Therefore, sampling in the spatial domain can be calculated from Eq. (8) as

$$\Delta x = \frac{\pi}{k_s} = \frac{\pi}{2k_0} = \frac{\lambda}{4} \tag{9}$$

In practice, the off-axis angle is lower than 90° and the sampling step can be slightly larger. Furthermore, overlapping degree varies depending on the type of reference antenna and the measured AUT. Directive antennas have narrower spectra [28] and the part of the spectrum associated to the squared signals often decays faster as it is computed for the convolution of two signals of bandwidth k_0 [5].

2.2. Modified hologram

The modified hologram technique was first employed for setups with radiated reference fields in Refs. [21, 38] and successively adapted for synthesized reference fields (see Section 2.3) in Refs. [27–29]. The technique consists in the removal of the autocorrelation terms of the hologram prior to the filtering process and can be implemented by means of two different approaches. First of them requires an extra measurement to characterize the amplitude of E_{aut} (the amplitude of E_{ref} is *a priori* known) [21, 23, 29, 30, 39]. Second approach, commonly known as *opposite-phase* holography [28, 40], introduces a *hybrid-T* component in the setup, which provides simultaneously the complete hologram in the sum port and the autocorrelation terms in the difference port. Another approach, used in imaging applications, is to increase the reference level several times above the level of the AUT's field in order to reduce the autocorrelation terms of the hologram [41, 42].

Thanks to the removal of the autocorrelation terms, separation between the image terms can be reduced, meaning that physical separation between the AUT and the reference antenna can also be reduced yielding the following advances:

- Overlapping is diminished and thus quality of the phase retrieval is improved.
- The extension of the *k*-space can also be reduced, involving larger sampling steps and less acquisition time [21, 28].
- Since the antennas can be placed close to each other and the off-axis angle can be reduced, the size of the setup is decreased and the paths of the reference and AUT fields are similar, resulting in less sensitive setups to scanning errors and source instability [21, 43].

Another advantage of this technique is that since the intensity of E_{aut} is measured, the final field can be composed with the measured amplitude and the retrieved phase rather than retrieving both, amplitude and phase, from the interferometric pattern as supposed so far. Thus, the quality of the phase retrieval is improved.

Main disadvantage for the modified hologram technique is that an extra measurement for the characterization of the amplitude of the AUT is required.

2.3. Synthesized reference field off-axis holography

Main differences between optical and microwave holography are stated in Ref. [27]. One of the most important remarks is that in microwave (and mm- and submm-wave bands) the hologram can be (coherently) recorded by scanning the probe across the acquisition plane, meaning that, instead of using radiated reference waves, they can be electronically synthesized and added to the field of the AUT.

Conventional approach to implement synthesized wave setups is schematically shown in **Figure 3**. A plane wave is synthesized by means of a phase shifter by cyclically modifying the phase of the sample of the field in the output of the directional coupler for each point of the acquisition plane. The synthesized wave is added to the acquired field of the AUT by means of a power combiner in the receiver's end.

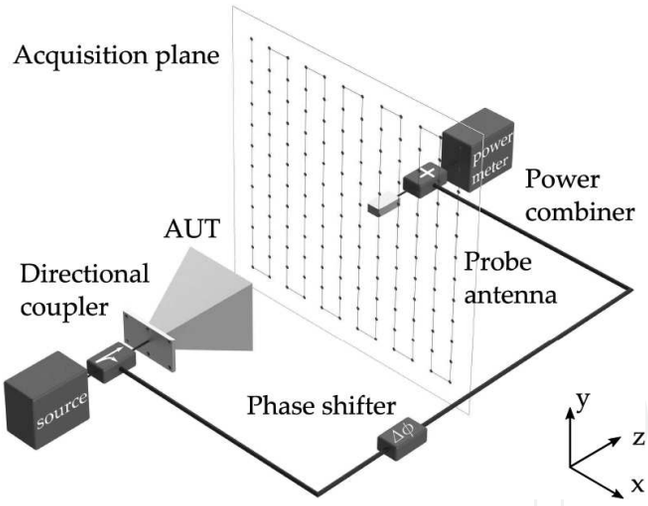

Figure 3. Conventional setup for synthesized wave off-axis holography.

In synthesized reference wave setups, position of the image terms is no longer related to the physical position of the reference antenna but to spatial sampling and the phase shifts $\Delta\phi$, between each point of the acquisition plane, and can be defined as:

$$k_{r,x} = \frac{\pm\Delta\phi}{\Delta x}. \tag{10}$$

The use of electrically synthesized waves removes the limitation imposed by the off-axis angle and makes possible to displace the image terms to the nonvisible part of the spectrum defined by $k_x^2 + k_y^2 < k_0^2$ [1].

Considering the nonoverlapping condition imposed in Eq. (7), the sampling step has to be selected depending on the value of the introduced phase shifts, which are typically selected as $\pi/2$, $2\pi/3$, or $3\pi/4$, yielding sampling steps of $\lambda/4$, $\lambda/6$, or $\lambda/8$, respectively [5, 28, 29].

This technique has several advantages:

- Overlapping can be controlled by selecting the phase shifts and the corresponding sampling rate.
- Modified hologram approaches can also be applied, thus sampling rate can also be relaxed.
- Since the reference wave is synthesized, it is not necessary to previously characterize it in amplitude and phase and its analytical expression can be employed in Eq. (5) for the phase retrieval. Hence, completely scalar acquisitions are made. Nevertheless, the nonideal behavior of the phase shifter and the rest of the components introduce modulations in the signal and, thus, its characterization is recommended [44].

However, synthesized reference field indirect off-axis holography also presents the following limitations:

- The sampling rate has to be increased in order to displace the image terms to the nonvisible part of the spectrum and to extend its limits. Thus, the acquisition time is increased and so it is the required system stability.
- The increased sampling step can also be a problem at mm- and submm-wave bands if too dense sampling grids are required, due to the positioning accuracy of the system.
- Two new components have to be included in the setup which can also pose a problem at high frequency bands due to the cost and complexity of those types of devices.

2.4. Main drawbacks and limitations of indirect off-axis holography

Despite the multiple advantages of conventional indirect off-axis techniques versus complex field measurements, such as robustness and cost reduction [21, 43], and also versus other amplitude-only techniques based on iterative approaches, conventional indirect off-axis techniques exhibit several limitations, which are summarized next:

- The reference field needs to be characterized in amplitude and phase at least once, and thus, the technique cannot be implemented only by means of scalar acquisitions since an initial vector calibration is required. Nevertheless, the use of synthesized waves [28, 29, 40] solves this problem, since the phase can be obtained analytically. Other methods to avoid the phase acquisition of the reference antenna such as the use of well-known antennas whose phase behavior can be modeled have also been proposed [21, 45].
- Setups based on synthesized waves solve the previous drawback and also allows to control overlapping of the image terms. However, implementation of this type of setups

involves the use of more radiofrequency (RF) components, i.e., phase shifters and power combiners. Implementation of these types of devices is not trivial at high frequency bands and the cost of the system can be highly increased.

- In addition, as shown in **Figure 3**, the reference signal has to be conveyed from the output of the directional coupler and phase shifter to the power combiner, located at the receiver's end. Nevertheless, high frequency equipment (e.g., over 110 GHz) usually requires the use of waveguide sections to convey the signal. In general, these waveguides cannot be arbitrarily bent. Other choice is to convey, by means of flexible cables, a low-frequency signal as reference and, at the end of the cable, resort to a frequency multiplier. However, this approach can suffer from phase inaccuracies due to cable flexing and temperature drift; also the use of frequency multipliers can increase the cost of the measurement system.
- The use of the modified hologram technique can alleviate the dense sampling demanded at the expenses of an extra measurement for the characterization of the amplitude of the AUT.
- Conventional indirect off-axis holography is a monochromatic technique. Thus, its use for broadband antennas characterization might be unfeasible if each frequency analysis requires an independent spatial acquisition.

Other phase retrieval approaches have been proposed in order to overcome the dense sampling requirements. In Refs. [41] and [46], a new approach, known as *phase-shifting*, derived from digital inline microscopy, employs three different holograms recorded after introducing phase shifts in the reference field to perform the phase retrieval in the spatial domain; in this case, the phase can be retrieved point-by-point. The method presented in Ref. [47] for a bistatic imaging setup can also be directly employed in antenna measurement setups. In this case, the phase retrieval is performed by solving a set of equations formed by the modified hologram expression and the expression that relates $\|E_{\text{aut}}(\vec{r})\|^2$ to its real and imaginary parts. For both cases the phase is retrieved directly in the spatial domain and, therefore, a sampling rate of $\lambda/2$ can be used. An added advantage is that there is no restriction in the position of the reference antenna.

3. Indirect off-axis holography with mechanical phase shifts

In order to overcome some of the above-mentioned limitations of conventional techniques, two methods allowing either to substitute the phase shifter for mechanical displacements or to control the position of the image terms in setups with radiated reference waves are described in this section.

3.1. Synthesized reference field by means of mechanical shifts

As mentioned before, main advantages of the use of synthesized reference waves are overlapping control of the image terms and that the reference field can be analytically obtained by means of a phase shifter from a sample of the field. Nevertheless, phase shifters can increase the cost of the measurement system or simply not be available for a specific frequency band.

The proposed method aims for the substitution of the phase shifter (see **Figure 3**) with mechanical displacements of the probe to create the interference-like pattern. The reference branch will provide a constant sample of the source added to the field recorded by the probe by means of a power combiner.

The expression of the hologram in Eq. (2) can be particularized for the case of using synthesized plane waves ($E_{\text{ref}}(\vec{r}) = Ae^{-jk_0 r}$) as:

$$H(\vec{r}) = |E_{\text{aut}}(\vec{r})|^2 + A^2 + AE_{\text{aut}}(\vec{r})e^{+jk_0 r} + AE^*_{\text{aut}}(\vec{r})e^{-jk_0 r}. \tag{11}$$

On the other hand, the recorded hologram, over a planar conventional acquisition grid, in the setup of **Figure 3**, when no phase shifter is employed, could be expressed in the following way:

$$H(\vec{r}) = |E_{\text{aut}}(\vec{r}) + C|^2, \tag{12}$$

where C is the constant reference level added to the power combiner.

If small mechanical displacements $\vec{d} = d\vec{r}/||\vec{r}||_2$ are added between each of the points of that conventional acquisition grid, the field of the AUT can be approximated in those new points, disregarding the amplitude variation and taking into account only the phase change by

$$E_{\text{aut}}(\vec{r} + \vec{d}) \approx E_{\text{aut}}(\vec{r})e^{-jk_0 d}. \tag{13}$$

For those new points, the hologram in Eq. (12) can be rewritten as in Eq. (14), yielding an equivalent expression to Eq. (11):

$$H(\vec{r} + \vec{d}) = |E_{\text{aut}}(\vec{r})e^{-jk_0 d} + C|^2 = |E_{\text{aut}}(\vec{r})|^2 + C^2 + CE_{\text{aut}}(\vec{r})e^{-jk_0 d} + CE^*_{\text{aut}}(\vec{r})e^{+jk_0 d}. \tag{14}$$

Therefore, if the mechanical displacements are selected so that the term $e^{-jk_0 d}$ in Eq. (13) introduces appropriate phase shifts, the use of phase shifters can be avoided.

The new grid will be a three-dimensional layered grid with as many layers as number of considered phase shifts $N_\phi = 2\pi/\Delta\phi$. N_ϕ is fixed together with the sampling rate to control the position of the image terms of the hologram, see Eq. (10), and of course, the *modified hologram* technique (Section 2.2) can also be applied.

Figure 4 shows two different views of the measurement grid generated for the experimental validation of the setup presented next. For those examples, the mechanical displacements are selected to introduce a phase shift of $\pi/2$ and thus, $N_\phi = 4$, as it can be clearly seen in **Figure 4(a)**. **Figure 4(b)** shows the top view of the grid in which the cyclically repeated pattern can be observed. The orange dots represent the top layer with regular sampling of $\lambda/2$, whereas the blue ones are those corresponding to the modified points introduced to generate the phase shifts, yielding a final sampling step of $\lambda/8$. The solid line interconnecting the dots indicates the sweep direction. The grid creation process can equivalently be seen as a modification of $N_\phi - 1$ of every N_ϕ points in the sweep axis of a regular grid to introduce the desired phase shifts.

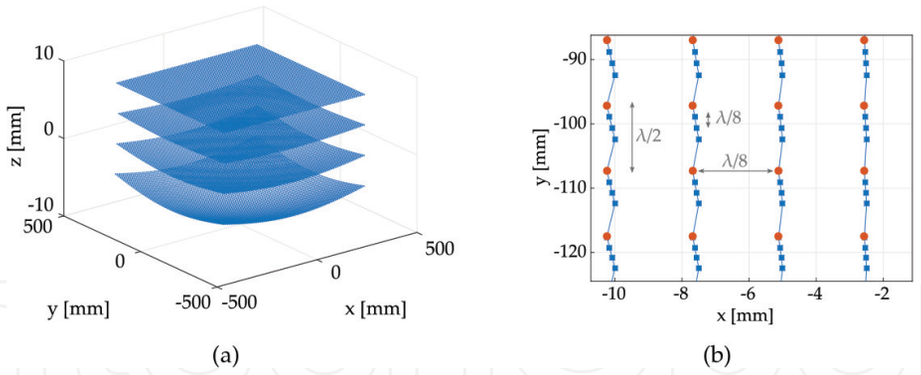

Figure 4. Three-dimensional acquisition grid for the proposed method. Note that a different scale has been used for all the axes: (a) complete grid and (b) detail of the top view.

For the phase retrieval, there are two different options: (i) either Eq. (4) is transformed back to the spatial domain and only the points corresponding to the top layer of the grid are selected, or (ii) the field is retrieved as in Eq. (5) analytically modeling the phase of the reference field. A compensation for the e^{+jk_0r} term introduced in the modified acquisition points (see Eq. (13)) has to be considered for the latter case.

Despite the approximation in Eq. (13), it is only valid in the FF of the AUT, the maximum phase shift that can be considered is π. This phase shift is associated to a displacement of $\lambda/2$, which does not have an influence in the amplitude level; therefore, as it will be proven in the experimental validation, the method provides good results when applied to NF acquisitions.

3.1.1. Experimental validation in the Ku-band for antenna measurement and diagnostics

A small 15 dB standard gain horn (SGH) antenna is characterized at 15 GHz. The measurements are repeated for the case in which a metallic plate blocks part of the antenna aperture as shown in **Figure 5**. In order to perform antenna diagnostics, in both cases, the retrieved field on the measurement plane is backpropagated to the aperture plane of the AUT. The setup is equivalent to those for imaging applications measured in transmission [41, 45].

The regular acquisition grid is a XY rectangular grid of 700 mm × 700 mm with 10 mm sampling ($\lambda/2$ at 15 GHz) in the y-axis and 2.5 mm ($\lambda/8$) in the x-axis, placed at $z_0 = 620$ mm of the aperture of the AUT. As $\pi/2$ phase shifts are being considered, three more layers of modified points, as shown in **Figure 4**, are considered, being the sampling step considering all the points in the y-axis also of $\lambda/8$.

If Eq. (10) is applied for the proposed configuration, the central position of the image terms is $\pm 2k_0$. **Figure 6(a)** shows the recorded NF hologram while its spectrum is shown in **Figure 6(b)**. Since the sweep (and the phase shifts) is made along the y-axis direction, the image terms will appear shifted in the k_y axis of the spectrum. The abrupt decay of the autocorrelation terms makes possible to correctly filter the desired image term between $0.4\,k_0$ and $3.6\,k_0$, and correctly retrieve the field of the AUT.

http://dx.doi.org/10.5772/67294

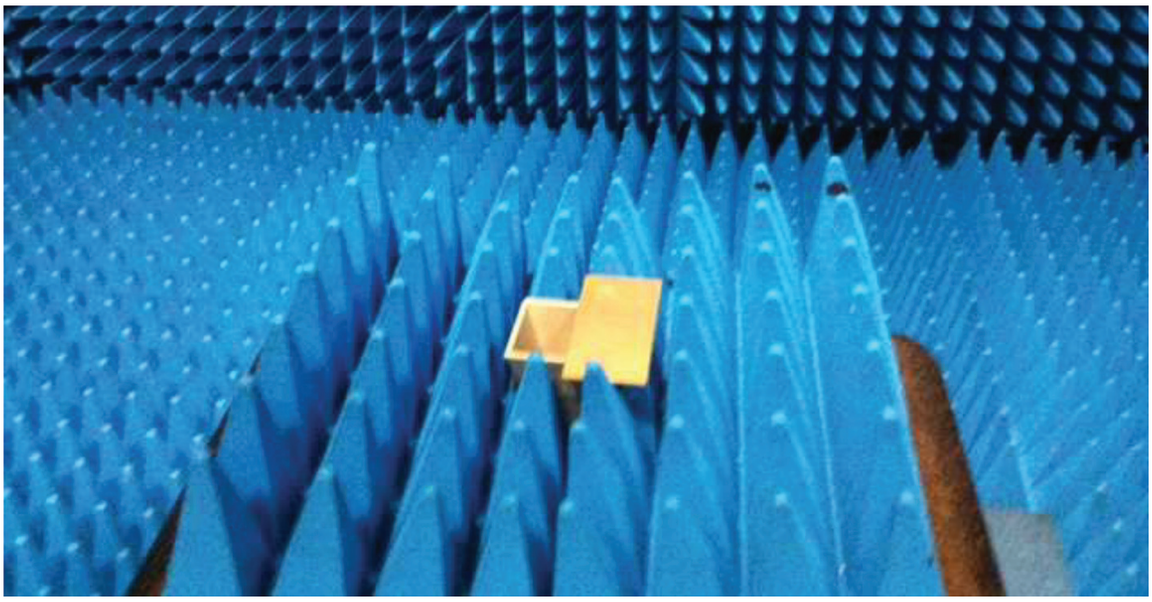

Figure 5. Ku band SGH with blocked aperture.

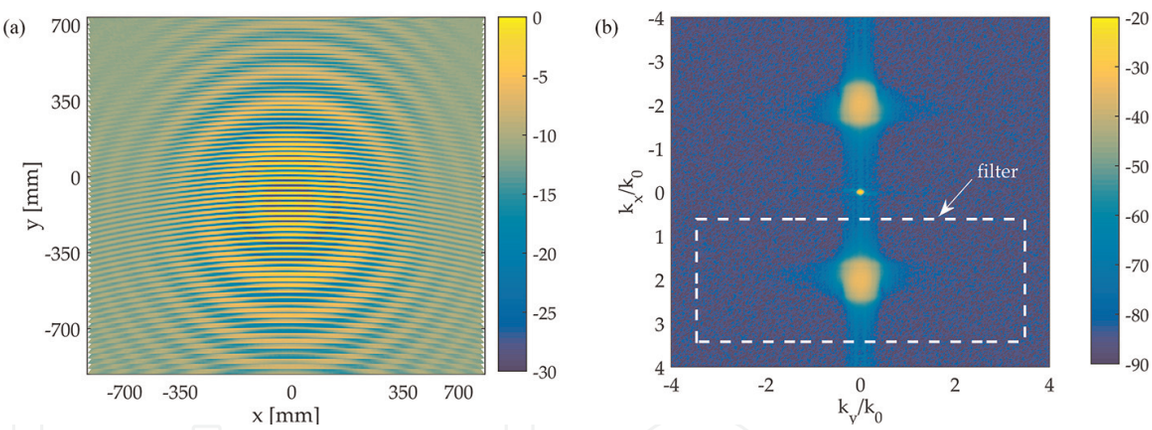

Figure 6. (a) Recorded hologram in the modified three-dimensional grid, normalized amplitude in dB. (b) Spectrum of the hologram, normalized amplitude in dB.

The retrieved amplitude and phase of the acquired NF are shown in **Figure7(a)** and, respectively, for the case in which the horn is not blocked. The backpropagated field in the aperture is shown in **Figure 7(c)** together with the size of the aperture. The retrieved amplitude and phase for the case of the blocked aperture are shown in **Figure 7(d)** and. Some discrepancies with respect to the first case can be observed and when the field is backpropagated to the aperture of the AUT, **Figure 7(f)**, the blockage can be clearly detected.

Thus, the proposed method can be successfully applied to antenna measurement and diagnostics with equivalent results to the conventional indirect off-axis method with synthesized reference wave.

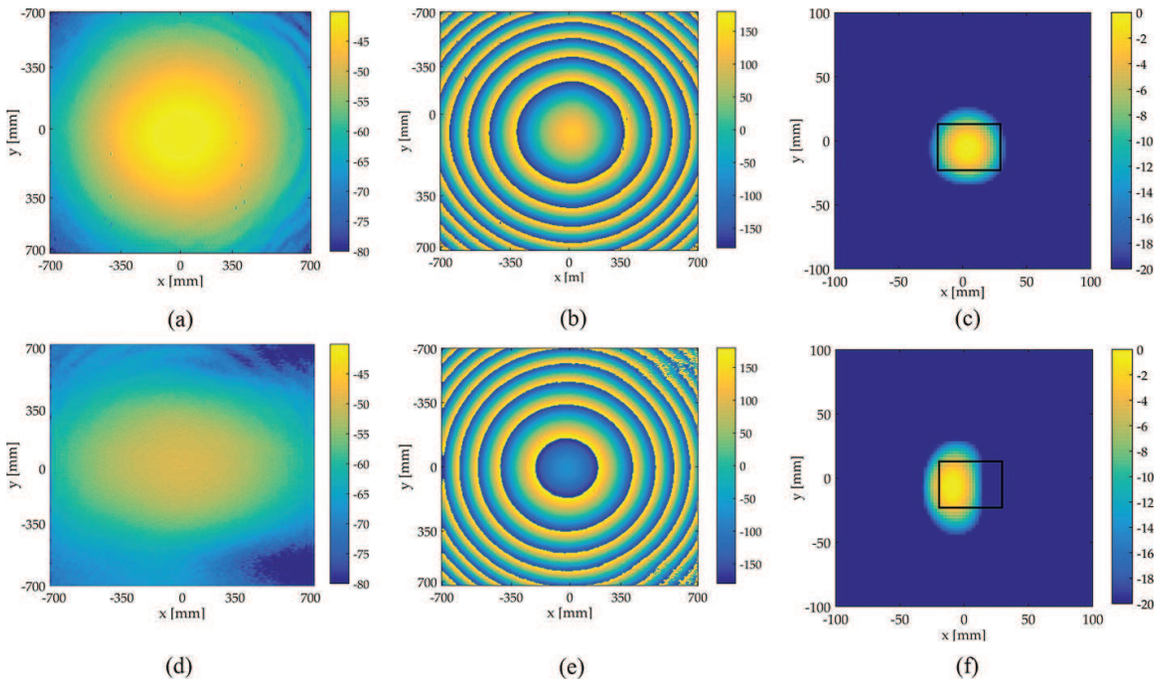

Figure 7. Retrieved NF of the AUT without blocking metallic plate (a)–(c) and with blocking metallic plate (d)–(f): (a) and (d) normalized amplitude in dB, (b) and (e) phase in degrees, and (c) and (f) backpropagation of the retrieved field toward the aperture, normalized amplitude in dB.

3.2. Multiplexed holograms with radiated reference field

As explained in Section 2.4, setups with synthesized reference waves for antenna characterization are challenging at high frequency bands, being necessary to resort to setups with radiated reference waves [21, 30]. The main limitation of these setups is that the position of the image terms is determined by the off-axis angle of the reference antenna, see Eq. (6), and will always be below $\pm k_0$, that is, in the visible part of the spectrum. This separation might not be enough to avoid overlapping for certain types of antennas such as nondirective antennas, which have wider spectra [28]. Overlapping can also be observed when the level in the AUT branch is higher than the reference level, due to the differences between the level of the autocorrelation and image terms [30].

The previously presented technique with mechanical phase shifts of the probe cannot be applied when radiated reference waves are employed because the displacements of the probe antenna will introduce the phase shifts in both the reference and the AUT fields, leading to an erroneous approach of the off-axis holography technique.

In order to control the position of the image terms and displace it to the nonvisible part of the spectrum as with synthesized reference waves, this subsection describes a new method for the case of using radiated reference waves. The method consists in multiplexing two subsampled holograms, Eq. (1), obtained from two 180° phase-shifted reference waves. The phase shift can be generated by means of a phase shifter or displacing the reference antenna a distance of $\lambda/2$.

http://dx.doi.org/10.5772/67294

The first subsampled hologram, blue grid in **Figure 8(a)**, is acquired in a grid with $2\Delta x$ and Δy sampling. The samples are stored in the odd columns of the multiplexed hologram. Then, a displacement of $\lambda/2$ is introduced in the reference antenna and the second subsampled hologram, which is stored in the even columns of the multiplexed hologram (orange grid in **Figure 8(b)**) is acquired over a grid identical to the first one but with an offset of Δx.

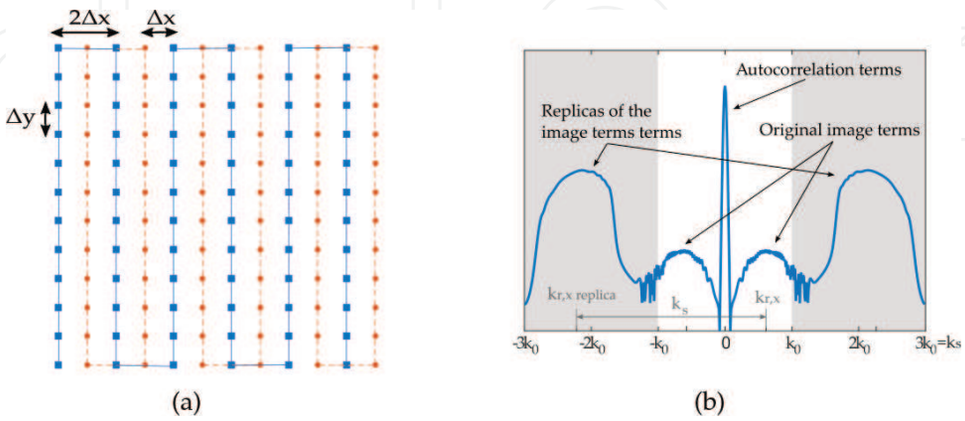

Figure 8. (a) Spatial multiplexation of the subsampled grids for the hologram formation. (b) Spectrum of the hologram for the proposed method for an example with $\Delta x = \lambda/6$ sampling.

By combining the two subsampled holograms with 180° phase-shifted references, the amplitude of the final hologram remains almost unchanged with respect to a hologram acquired in the complete grid, while the phase steps of the reference field ($\Delta\phi$) in the acquisition plane will be increased by a factor of π (see Ref. [30] for a step-by-step proof), leading to the following position of the image terms (see Eqs. (8) and (10)):

$$k'_r = \pm\frac{\Delta\phi + \pi}{\Delta x} = \pm\frac{\Delta\phi}{\Delta x} + \frac{\pi}{\Delta x} = \pm k_r + k_s. \tag{15}$$

Two replicas of the image terms of the hologram appear at a distance of $k_s = \frac{\pi}{\Delta x}$ of the original image terms as shown in **Figure 8(b)**. The replicas are in the nonvisible part of the spectrum, shaded in gray, and have the same information than the original image terms, which are overlapped with the autocorrelation terms. Hence, the field can be retrieved by filtering the desired replica without the need to resort to the modified hologram technique. It has been demonstrated that if the reference field is a plane wave, the original terms are completely canceled allowing a cleaner filtering [30].

Position of the image terms depends on the off-axis angle of the reference antenna, Eq. (6). A common option to convey the reference signal in holography setups is to use mirror reflection (see **Figure 9**). This option has multiple advances since it is possible to increase the path of the reference field and interfere with a quasi-plane wave. Furthermore, by modifying the position and orientation of the reflector it is possible not only to control the off-axis angle but also to modify the shape of the pattern of the reference field in the acquisition plane, which also influences the shape and the width of the image terms and their replicas in the *k*-space.

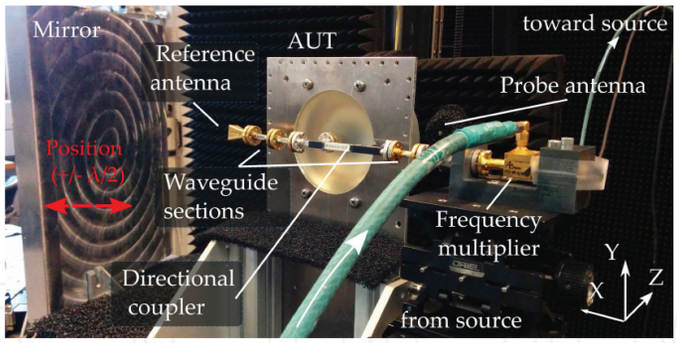

Figure 9. Measurement setup for the lens antenna characterization at 94 GHz. Rear view.

3.2.1. Corrections

Two small corrections have to be applied to the retrieved field to compensate the effect that the high frequency replicas introduce in the retrieved field. First, the retrieved phase is contaminated with high frequency noise that can be eliminated by low-pass filtering. Second, since only a fraction of the spectral density of the image term is being considered (the replica), the retrieved amplitude of the AUT is slightly smaller than the one directly acquired. A correction factor can be obtained from the analysis of the reference field, which is known. The spectrum of the reference field is filtered using the same filter that will be used to filter the image term of the complete hologram; then, that filtered part is transformed back to the spatial domain and its amplitude level is compared to the initial amplitude of the reference field. The difference can be used as a correction factor for the retrieved amplitude of the AUT.

3.2.2. Experimental validation: 94 GHz lens antenna NF characterization

The measurement setup shown in **Figure 9** has been implemented for the experimental validation of the method. A 64 mm circular lens fed with a horizontally polarized WR10 open-ended waveguide (OEWG) is characterized at 94 GHz. A 20 dB SGH is employed as reference antenna. A plane metallic mirror with a tilt of 22° is placed at 270 mm of the aperture of the reference antenna and used to direct the reference field toward the acquisition plane, at 200 mm of the AUT.

The NF is acquired for a 200 mm cut at $y = 0$ with $\lambda/2$ sampling for the first position of the mirror. Then, the mirror is displaced $\lambda/2$ toward the acquisition plane by means of a micropositioner and the second subsampled hologram is acquired. Direct acquisition of the phase and acquisition with conventional off-axis holography with $\lambda/4$ sampling have also been made to compare the results to those obtained with the proposed method.

Figure 10(a) shows the hologram for the proposed method and for conventional indirect off-axis holography. An off-axis angle of 22° produces two image terms centered in $\pm 0.38k_0$ and two replicas at $\mp 2.38k_0$, which means that, in the $[-2k_0, 2k_0]$ interval, the replicas are swapped and centered at $\mp 1.64k_0$, as it can be clearly seen. While the replicas for the proposed method can be filtered, there is some overlapping between the image term and the autocorrelation terms for the conventional case. This is due to the high amplitude level of the AUT, which produces a large autocorrelation term, highly above the level of the image terms of the spectrum.

http://dx.doi.org/10.5772/67294

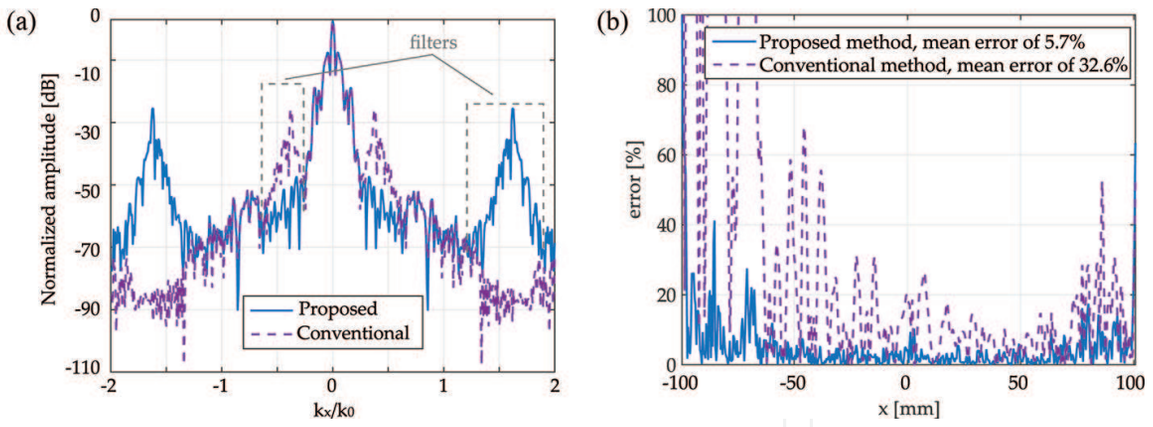

Figure 10. (a) Spectrum of the hologram and filtering windows, normalized amplitude in dB and (b) percentual error of the phase retrieval.

Figure 10(b) depicts the error of the phase retrieval process calculated as

$$error[\%] = 100\,\frac{\|\mathbf{E}_{\mathbf{measured}} - \mathbf{E}_{\mathbf{retrieved}}\|_2}{\|\mathbf{E}_{\mathbf{measured}}\|_2}, \tag{16}$$

where $\mathbf{E}_{\mathbf{measured}}$ and $\mathbf{E}_{\mathbf{retrieved}}$ are vectors containing the samples of the measured (with amplitude and phase) and the retrieved field (from amplitude-only acquisitions) at the acquisition points, and $\|\cdot\|_2$ denotes the Euclidean norm. Due to the overlapping with the autocorrelation term, the mean error of the conventional method is 32.8% while the error achieved with the proposed method is only of 5.70%.

Figure 11(a) shows the retrieved amplitude in the acquisition plane with both methods compared to the amplitude directly acquired, whereas in **Figure 11(b)** the same data are shown for the phase. It can be clearly observed that, while with the proposed method, the retrieved amplitude and phase are in very good agreement with the data from the direct acquisition the retrieved fields with the conventional method exhibit some discrepancies, especially in the areas with larger error (see **Figure 10(b)**) due to the overlapping of the spectrum.

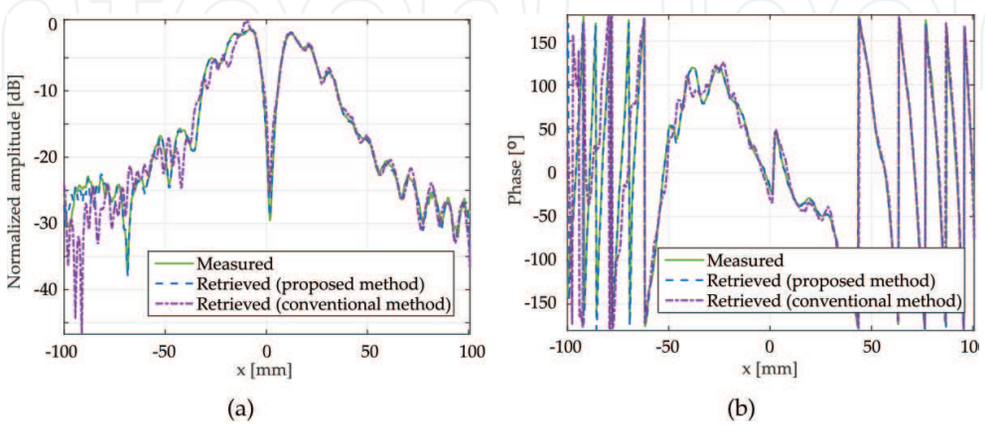

Figure 11. (a) Amplitude of the AUT, normalized in dB and (b) phase of the AUT in degrees.

4. Broadband indirect off-axis holography

Previous techniques are monochromatic techniques that might not be suitable for characterization of broadband antennas, for whose measurement it is usual to resort to time-domain (TD) techniques [48, 49].

The herein presented technique is an extrapolation of conventional off-axis holography that allows for efficient characterization of broadband antennas by means of amplitude-only acquisitions. Although the data acquisition and phase retrieval are different to the previous methods, as they are carried out in the TD, the physical layout of the elements is identical to the one already presented in **Figure 1**. This layout is presented in **Figure 12(a)** again in order to define some relevant distances that will be discussed later.

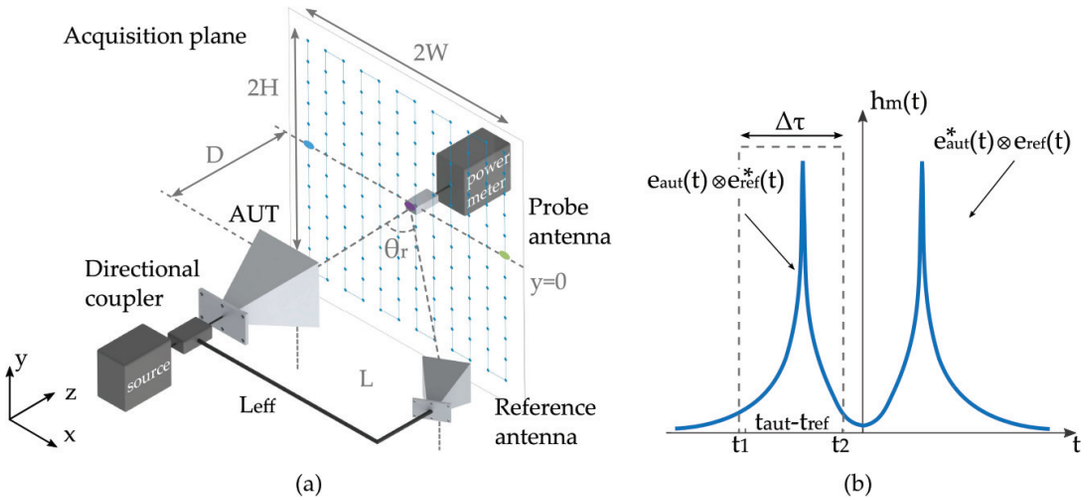

Figure 12. Broadband indirect off-axis holography: (a) layout of the measurement setup and (b) spectrum of the modified hologram.

During the acquisition process, a frequency sweep is made for each point of the spatial grid and the hologram is acquired over the studied frequency band, Eq. (17); then the spectrum is computed in the TD by means of an inverse FT, Eq. (18):

$$H(\vec{r},\omega) = |E_{\text{aut}}(\vec{r},\omega)|^2 + |E_{\text{ref}}(\vec{r},\omega)|^2 + E_{\text{aut}}(\vec{r},\omega)E^*_{\text{ref}}(\vec{r},\omega) + E^*_{\text{aut}}(\vec{r},\omega)E_{\text{ref}}(\vec{r},\omega) \tag{17}$$

$$h(\vec{r},t) = |e_{\text{aut}}(\vec{r},t)|^2 + |e_{\text{ref}}(\vec{r},t)|^2 + e_{\text{aut}}(\vec{r},t) \otimes e^*_{\text{ref}}(\vec{r},t) + e^*_{\text{aut}}(\vec{r},t) \otimes e_{\text{ref}}(\vec{r},t) \tag{18}$$

After filtering the desired image term in the TD by means of a time window Π, defined from t_1 to t_2:

$$h_{\text{filtered}}(\vec{r},t) = \Pi(t_1,t_2)\{e_{\text{aut}}(\vec{r},t) \otimes e^*_{\text{ref}}(\vec{r},t)\}, \tag{19}$$

the phase retrieval is performed at each spatial point, simultaneously for all the acquired frequencies as

$$E_{\text{aut,retrieved}}(\vec{r},\omega) = \frac{FT_t\{h_{\text{filtered}}(\vec{r},t)\}}{E^*_{\text{ref}}(\vec{r},\omega)}. \tag{20}$$

The subindex t in the FT indicates that the spectrum is computed in the TD.

This allows to retrieve one of the components of the tangential field in the acquisition plane, in order to obtain the FF of the AUT, as in the previous methods, the second tangential component also needs to be retrieved for NF-FF transformation. To do that, the process has to be repeated after a turn of 90° of the AUT to change the acquired polarization.

Main advantages of this method are that position of the image terms can be controlled with the distance between the AUT and the reference antenna, the physical length of the AUT and reference branches, and the separation between the antennas and the acquisition plane, as it will be addressed next. Furthermore, as the phase is retrieved point-by-point in the spatial grid, the technique is compatible with array thinning techniques that allow to drastically reduce the number of acquisition points with the consequent time reduction [22, 31, 50].

On the other hand, the method also presents some disadvantages. As in conventional indirect off-axis holography, the reference antenna has to be previously known in amplitude and phase, also all the components of the setup, mainly the AUT, must be broadband; otherwise their time responses will be spread and may cause overlapping in the spectrum of the recorded hologram [23].

4.1. Main parameter constraints

As in the previous methods, quality of the retrieved fields depends on how clean the filtering process is. Since the spectrum of the hologram is computed in the TD, position of the image terms is dependent on the starting times of the signals coming from the AUT t_{aut} and from the reference antenna t_{ref}, and thus, it can be controlled with the distance and the length L_{eff} of the transmission lines employed in the setup.

In order to avoid overlapping two main restrictions have to be fulfilled:

- The length of the elements in the reference branch must be selected so that the image terms of the spectrum are swapped, $t_{\text{aut}} - t_{\text{ref}} + \Delta\tau < 0$. Thus, the desired term can be easily filtered, as shown in **Figure 12(b)**.

  In terms of the distances between elements in the setup, as defined in **Figure 12(a)**, the previous condition yields the following expression considering the worst-case scenario (points in the corners of the acquisition plane closer to the reference antenna for whose $t_{\text{ref}} > t_{\text{aut}}$):

$$\sqrt{D^2 + W^2 + H^2} - (\sqrt{D^2 + (W - L)^2 + H^2} + L_{\text{eff}}) + c\Delta\tau < 0, \tag{21}$$

$$L_{\text{eff}} - L > c\Delta\tau. \tag{22}$$

- The frequency sampling must be selected according to the *Nyquist* rule:

$$\Delta f < \frac{1}{2T} = \frac{1}{2(t_{\text{ref}} - t_{\text{aut}})}. \tag{23}$$

4.2. Numerical validation for the characterization of a horn antenna in the Ka-band

For the numerical validation of the method, a 25 dB SGH is characterized in the Ka-band from 26.5 to 40 GHz. The physical layout is shown in **Figure 13**. The acquisition plane is a square grid of 300 mm side with spatial sampling of 3.7 mm in both directions, that is, $\lambda/2$ at 40 GHz, and is located at a distance of $D = 260$ mm of the aperture of the AUT. A 15 dB horn is employed as reference antenna placed at $L = 200$ mm from the center of the aperture of the AUT with an off-axis angle of $\theta_r = 37.5^{\circ}$. A coaxial cable of $L_{\text{eff}} \approx 48$ cm is employed to connect the directional coupler to the reference antenna.

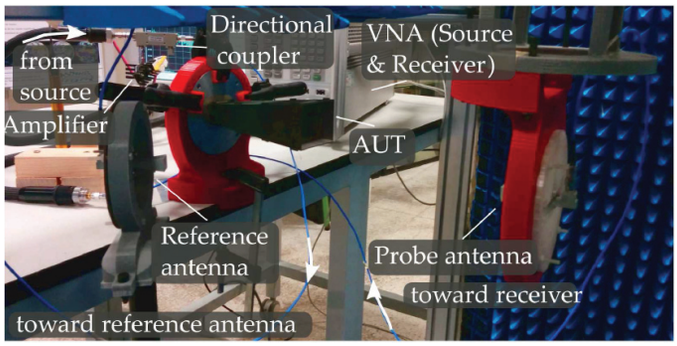

Figure 13. Setup for the 25 dB SGH antenna characterization in the Ka-band.

Figure 14(a) shows the modified hologram for the three points highlighted in **Figure 12(a)**. The position of the image terms varies depending on the position of the probe in the acquisition plane. **Figure 14(b)** shows a detail of the retrieved phase in the central part of the frequency band for the worst-case scenario. Apart from some 180° phase shifts, the agreement between the retrieved and directly measured phase is almost complete. Finally, **Figure 14(c)** depicts the error computed as in Eq. (16). Mean value of the error in the complete frequency band is 2.24%. The large values above 37 GHz are due to the signal level of the reference antenna, which decays in that part of the band.

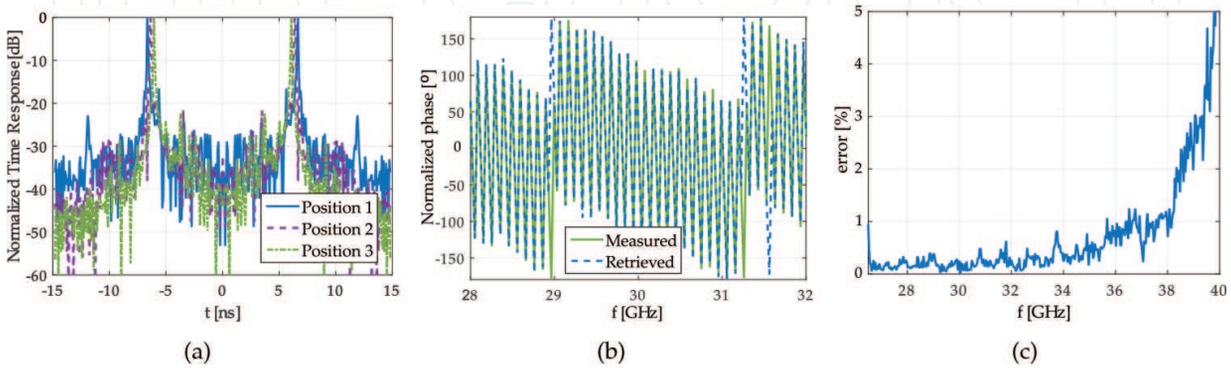

Figure 14. Phase retrieval process: (a) spectrum of the modified hologram for three different acquisition points, (b) detail of the retrieved phase in the central frequency band, and (c) error for the phase retrieval in the complete frequency band.

http://dx.doi.org/10.5772/67294

The retrieved phase in the acquisition plane at 30 GHz is shown in **Figure 15** compared to the phase directly acquired at that frequency. For this frequency, the error of the phase retrieval is 0.25%; thus, the retrieved phase is practically identical to the measured one.

After the phase is retrieved simultaneously for all the frequencies at each point of the acquisition plane, conventional NF-FF transformation and backpropagation techniques can be applied for the computation of the FF pattern and the fields in the aperture of the AUT [1]. **Figure 15(a)** shows the copolar pattern of the FF at 30 GHz, while the E_x component of the field in the aperture is shown in **Figure 15(b)**. The black rectangle depicts the position of the aperture whose size is 700 mm × 500 mm.

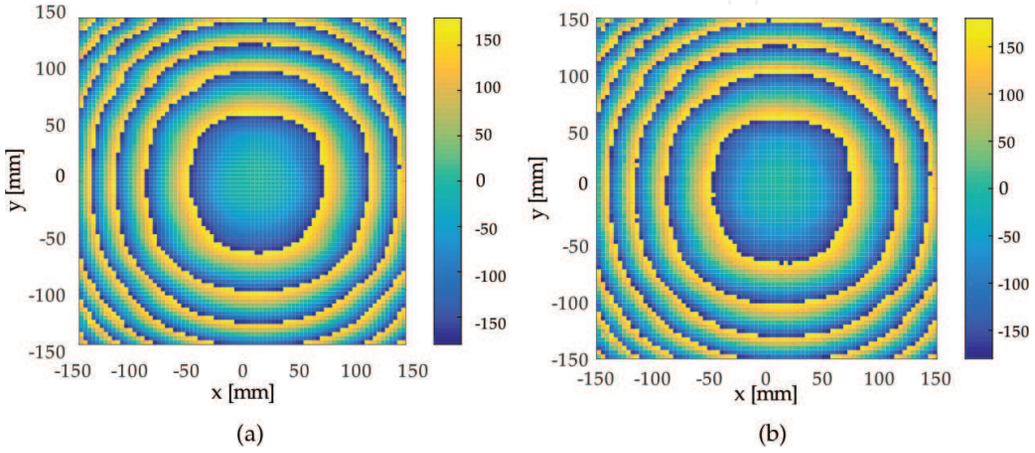

Figure 15. Retrieved phase of the AUT at 30 GHz compared to the direct measurement: (a) directly acquired phase in the NF, degrees, and (b) retrieved phase, degrees.

Finally, **Figure 16** shows the main cuts for $\phi = 0°$ and $\phi = 90°$ of the copolar pattern in **Figure 15(a)** (blue line labeled as *Retrieved NF*) compared to the cuts of a direct FF acquisition in an spherical anechoic chamber (labeled as *Measured FF*) and the cuts obtained for a NF-FF transformation of a field acquired with amplitude and phase (labeled as *Measured NF*). The valid margin of the NF-FF transformation, in which the data are comparable, is ±25° [1]. High level of coincidence

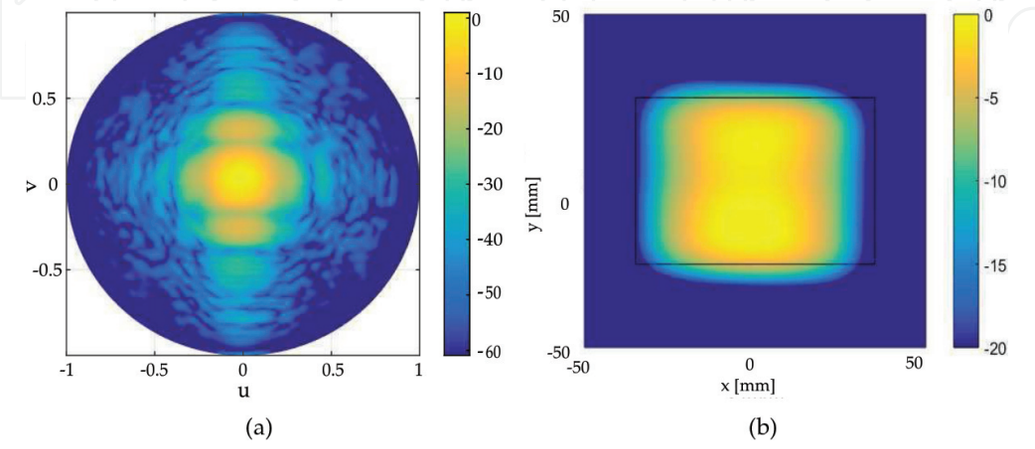

Figure 16. AUT characterization at 30 GHz from the retrieved data: (a) normalized FF copolar pattern in dB and (b) normalized E_x component of the field in the aperture of the AUT in dB.

can be observed between the three measurements. The small differences between the data directly acquired in FF and the transformed data are attributed to the lack of application of probe correction techniques during the NF-FF transformation (**Figure 17**) [1].

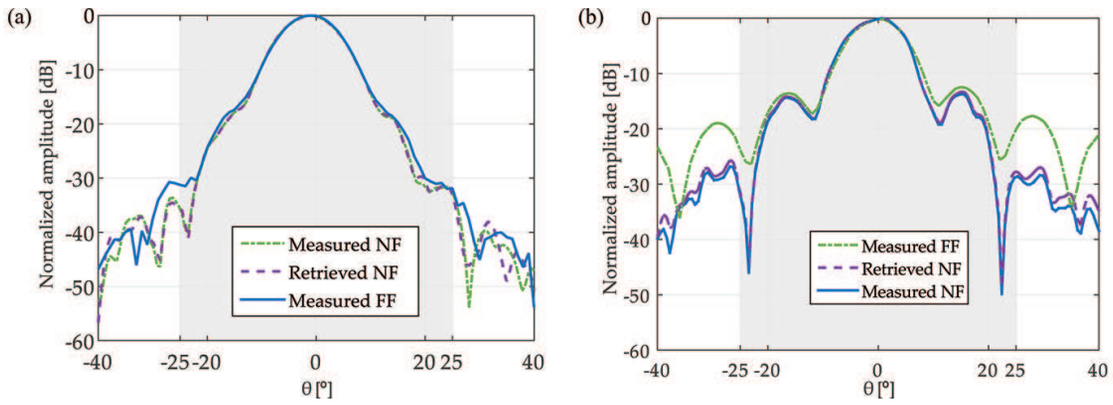

Figure 17. Comparison of the main cuts of the normalized amplitude of the AUT: (a) $\phi = 0^{\circ}$ and (b) $\phi = 90^{\circ}$. The gray shaded areas indicate the valid margin of the NF-FF transformation [23].

5. Conclusion

Indirect off-axis holography is a method that allows for phase retrieval of an unknown field from amplitude-only acquisitions. This technique has been widely employed for antenna measurement and diagnostics for which phase acquisition is challenging, especially at high frequency bands, where very accurate positioning and high environmental stability are required.

Several modifications such as the *modified hologram* technique and the use of *synthesized reference waves* have been discussed, in order to overcome known disadvantages of the conventional technique regarding the required sampling rates or the spectral overlapping issues. Nevertheless, even with these modifications, indirect off-axis holography exhibits some limitations, and thus, three novel methods developed in order to overcome them are proposed.

Two of the presented techniques employ mechanical shifts, the first one to avoid the use of phase shifters and reduce the cost of the measurement system, and the second to control the position of the image terms in the same way that it is controlled with synthesized reference waves but with radiated reference fields. This enables to apply synthesized reference-like techniques in high frequency bands. The last technique is an extrapolation of the conventional technique employed for efficient phase retrieval of broadband antennas in which the phase is retrieved point-by-point in the acquisition plane and simultaneously for all frequency bands, by filtering the hologram in the TD instead of the *k*-space. **Table 1** summarizes the main advantages

and disadvantages of the conventional and novel indirect off-axis techniques employed for antenna metrology.

Experimental validation has been presented for each of the proposed methods with very good agreement with the reference results obtained from acquisitions performed directly with amplitude and phase.

Method	Advantages	Disadvantages
Conventional [24–26]	Amplitude-only measurement (applicable to all methods)	Complex characterization: $E_{\text{ref}}(\vec{r})$ Image terms: visible part of the spectrum
Modified hologram [5, 21, 23]	No autocorrelation terms: overlapping reduction	Extra acquisition: $\lvert E_{\text{aut}}(\vec{r})\rvert^2$
	Less dense sampling than conventional technique	
	Only phase retrieved: $\lvert E_{\text{aut}}(\vec{r})\rvert$ is measured	
Synthesized reference [27, 28, 43, 44]	Image terms: nonvisible region	More dense sampling
	Further overlapping reduction that modified hologram	Not implementable at high frequency bands with waveguide sections
	No need to measure $E_{\text{ref}}(\vec{r})$: scalar acquisition	
Mechanical phase shifts [5]	No phase shifter	Three-dimensional positioner
	The other advantages and disadvantages are the same as in *Synthesized reference*	
Multiplexed holograms [30]	Image terms in the nonvisible region	
	Radiated reference fields	Need of quasi-planar reference field,
	Implementable at high frequency bands	the path of the reference field has to be
	Less dense sampling than *Synthesized reference*	increased (higher sensitivity to errors)
Broadband holography [23, 31]	Efficient broadband characterization	Acquisition: frequency sampling capabilities
	Standard antenna measurement sampling ($\lambda/2$)	
	Phase retrieval point-by-point	

Table 1. Main features of the presented indirect off-axis holography techniques for antenna metrology.

Acknowledgements

This work has been partially supported by the Ministerio de Ciencia e Innovación of Spain/FEDER under projects TEC2014-55290-JIN (PortEMVision) and TEC2014-54005-P (MIRIIEM); by the Gobierno del Principado de Asturias through PCTI 2013-1017 GRUPIN14-114 and by grant LINE 525-002; and by the Academy of Finland through DYNAMITE project. The authors would like to thank M.Sc. Luis Díaz for his help with 3D modeling.

Author details

Ana Arboleya[1]*, Jaime Laviada[1], Juha Ala-Laurinaho[2], Yuri Álvarez[1], Fernando Las-Heras[1] and Antti V. Räisänen[2]

*Address all correspondence to: aarboleya@tsc.uniovi.es

1 Departamento de Ingeniería Eléctrica, Escuela Politécnica de Ingeniería, Universidad de Oviedo, Gijón, Spain

2 Department of Radio Science and Engineering and MilliLab, Aalto University, Espoo, Finland

References

[1] A.D. Yaghjian. An overview of near-field antenna measurements. *IEEE Trans. Antennas Propag*., 34(1):30–45, Jan. 1986.

[2] M.S. Castaner, A. Munoz-Acevedo, F. Cano-Fácila, and S. Burgos. Overview of novel post-processing techniques to reduce uncertainty in antenna measurements. In Md. Zahurul Haq, editor, *Advanced Topics in Measurements*, Chapter 9. Intech, 2012.

[3] F. Las-Heras and T.K. Sarkar. A direct optimization approach for source reconstruction and NF-FF transformation using amplitude-only data. *IEEE Trans. Antennas Propag*., 50 (4):500–510, Apr. 2002.

[4] C. Cappellin, A. Frandsen, S. Pivnenko, G. Lemanczyk, and O. Breinbjerg. Diagnostics of the SMOS radiometer antenna system at the DTU-ESA spherical near-field antenna test facility. In *2007 2nd European Conf. on Antennas and Propag. (EuCAP)*, pages 1–6, Edinburgh, UK, Nov. 2007.

[5] J. Laviada Martínez, A. Arboleya-Arboleya, Y. Álvarez López, C. García-González, and F. Las-Heras. Phaseless antenna diagnostics based on off-axis holography with synthetic reference wave. *IEEE Antennas Wireless Propag. Lett*., 13:43–46, 2014.

[6] B. Fuchs, L.L. Coq, and M.D. Migliore. Fast antenna array diagnosis from a small number of far-field measurements. *IEEE Trans. Antennas Propag*., 64(6):2227–2235, Jun. 2016.

[7] C.A. Balanis. *Antenna Theory: Analysis and Design*. John Wiley Sons, 2nd edition, New York, 1997.

[8] Std 521-2002 (revision of IEEE std 521-1984). IEEE standard letter designations for radar-frequency bands. Technical report, Institute of Electrical and Electronics Engineers, 2003.

[9] Y. Álvarez, F. Las-Heras, and C. García. The sources reconstruction method for antenna diagnostic and imaging applications. In Prof. Ahmed Kishk, editor, *Solutions and Applications of Scattering, Propagation, Radiation and Emission of Electromagnetic Waves*, Chapter 6. Intech, 2012.

[10] Y. Rahmat-Samii, V. Galindo-Israel, and R. Mittra. A plane-polar approach for far-field construction from near-field measurements. *IEEE Trans. Antennas Propag*., 28(2):216–230, Mar. 1980.

[11] F. D'Agostino, F. Ferrara, C. Gennarelli, R. Guerriero, and M. Migliozzi. An effective NF-FF transformation technique with planar spiral scanning tailored for quasi-planar antennas. *IEEE Trans. Antennas Propag*., 56(9):2981–2987, Sept. 2008.

[12] J.J.H. Wang. An examination of the theory and practices of planar near-field measurement. *IEEE Trans. Antennas Propag*., 36(6):746–753, Jun. 1988.

[13] S. Gregson, J. McCormick, and C. Parini. *Principles of Planar Near-field Antenna Measurements. Electromagnetic Waves*. Institution of Engineering and Technology (IET), London, 2007.

[14] A.C. Newell. Error analysis techniques for planar near-field measurements. *IEEE Trans. Antennas Propag*., 36(6):754–768, Jun. 1988.

[15] IEEE recommended practice for near-field antenna measurements. *IEEE Std 1720-2012*, pages 1–102, Institute of Electrical and Electronics Engineers, Dec. 2012.

[16] J. Säily, P. Eskelinen, and A.V. Räisänen. Pilot signal-based real-time measurement and correction of phase errors caused by microwave cable flexing in planar near-field tests. *IEEE Trans. Antennas Propag*., 51(2):195–200, Feb. 2003.

[17] J.A. Gordon, D.R. Novotny, M.H. Francis, R.C. Wittmann, M.L. Butler, A.E. Curtin, and J.R. Guerrieri. Millimeter-wave near-field measurements using coordinated robotics. *IEEE Trans. Antennas Propag*., 63(12):5351–5362, Dec. 2015.

[18] L.J. Foged, G. Barone, and F. Saccardi. Antenna measurement systems using multi-probe technology. In *2015 IEEE Conf. on Antenna Measurements Applications (CAMA)*, pages 1–3, Chiang Mai, Thailand, Nov. 2015.

[19] Y. Álvarez, F. Las-Heras, and M.R. Pino. The sources reconstruction method for amplitude-only field measurements. *IEEE Trans. Antennas Propag*., 58(8):2776–2781, Aug. 2010.

[20] M.D. Migliore and G. Panariello. A comparison of interferometric methods applied to array diagnosis from near-field data. *IEE Proc. Microwaves Antennas Propag*., 148(4):261–267, Aug. 2001.

[21] G. Junkin, T. Huang, and J.C. Bennett. Holographic testing of terahertz antennas. *IEEE Trans. Antennas Propag*., 48(3):409–417, Mar. 2000.

[22] J. Laviada and F. Las-Heras. Phaseless antenna measurement on non-redundant sample points via Leith-Upatnieks holography. *IEEE Trans. Antennas Propag*., 61(8):4036–4044, Aug. 2013.

[23] A. Arboleya, J. Laviada, J. Ala-Laurinaho, Y. Álvarez, F. Las-Heras, and A.V. Räisänen. Phaseless characterization of broadband antennas. *IEEE Trans. Antennas Propag*., 64(2):484–495, Feb. 2016.

[24] E.N. Leith and J. Upatnieks. Reconstructed wavefronts and communication theory. *J. Optical Soc. Am.*, 52(10):1123–1128, Oct. 1962.

[25] P.J. Napier and R.H.T. Bates. Antenna - aperture distributions from holographic type of radiation-pattern measurement. *Proc. Inst. Elect. Eng.*, 120(1):30–34, Jan. 1973.

[26] J.C. Bennett, A.P. Anderson, P. McInnes, and A.J.T. Whitaker. Microwave holographic metrology of large reflector antennas. *IEEE Trans. Antennas Propag.*, 24(3):295–303, May 1976.

[27] G.A. Deschamps. Some remarks on radio-frequency holography. *Proc. IEEE*, 55(4):570–571, Apr. 1967.

[28] M.P. Leach, D. Smith, S.P. Skobelev, and M. Elsdont. An improved holographic technique for medium-gain antenna near field measurements. In *2007 2nd European Conf. on Antennas and Propag. (EuCAP)*, pages 1–6, Edinburgh, UK, Nov. 2007.

[29] V. Schejbal, V. Kovarik, and D. Cermak. Synthesized-reference-wave holography for determining antenna radiation characteristics. *IEEE Antennas Propag. Mag.*, 50(5):71–83, Oct. 2008.

[30] A. Arboleya, J. Ala-Laurinaho, J. Laviada, Y. Álvarez, F. Las-Heras, and A.V. Räisänen. Millimeter-wave phaseless antenna measurement based on a modified off-axis holography setup. *J. Infrared Millimeter Terahertz Waves*, 37(2):160–174, 2016.

[31] A. Arboleya, J. Laviada, J. Ala-Laurinaho, Y. Álvarez, F. Las-Heras, and A.V. Räisänen. Reduced set of points in phaseless broadband near-field antenna measurement: Effects of noise and mechanical errors. In *2016 10th European Conf. on Antennas and Propag. (EuCAP)*, pages 1–5, Davos, Switzerland, Apr. 2016.

[32] A. Arboleya, Y. Álvarez, and F. Las-Heras. Millimeter and submillimeter planar measurement setup. In *2013 IEEE Antennas and Propag. Soc. Int. Symp. (APSURSI)*, pages 1–2, Orlando, FL, Jul. 2013.

[33] A.V. Räisänen, J. Ala-Laurinaho, A. Karttunen, J. Mallat, A. Tamminen, and M. Vaaja. Measurements of high-gain antennas at THz frequencies. In *2010 4th European Conf. on Antennas and Propag. (EuCAP)*, pages 1–3, Barcelona, Spain, Apr. 2010.

[34] D. Gabor. Microscopy by reconstructed wave-fronts. *Proc. R. Soc. London A: Math., Phys. Eng. Sci.*, 197(1051):454–487, Jul. 1949.

[35] A.P. Anderson. Microwave holography. *Proc. Inst. Elect. Eng.*, 124(11):946–962, Nov. 1977.

[36] G. Tricoles and N.H. Farhat. Microwave holography: Applications and techniques. *Proc. IEEE*, 65(1):108–121, Jan. 1977.

[37] A.V. Räisänen and J. Ala-Laurinaho. Holographic principles in antenna metrology at millimeter and submillimeter wavelengths. In *2015 9th European Conf. on Antennas and Propag. (EuCAP)*, pages 1–2, Lisbon, Portugal, Apr. 2015.

[38] P.H. Gardenier. *Antenna Aperture Phase Retrieval*. PhD thesis, Electrical and Electronic Engineering School, University of Canterbury, Christchurch, New Zealand, Apr. 1980.

[39] P.J. Napier. *Reconstruction of Radiating Sources*. PhD thesis, Electrical and Electronic Engineering School, University of Canterbury, Christchurch, New Zealand, Apr. 1971.

[40] D. Smith, M. Leach, M. Elsdon, and S.J. Foti. Indirect holographic techniques for determining antenna radiation characteristics and imaging aperture fields. *IEEE Mag. Antennas Propag.*, 49(1):54–67, Feb. 2007.

[41] J. Marín García. *Off-axis Holography in Microwave Imaging Systems*. PhD thesis, Departament de Telecomunicació i Enginyeria de Sistemes, Universitat Autònoma de Barcelona, 2015.

[42] M.S. Heimbeck, M.K. Kim, D.A. Gregory, and H.O. Everitt. Terahertz digital holography using angular spectrum and dual wavelength reconstruction methods. *Opt. Express*, 19 (10):9192–9200, May 2011.

[43] V. Schejbal, J. Pidanic, V. Kovarik, and D. Cermak. Accuracy analyses of synthesized-reference-wave holography for determining antenna radiation characteristics. *IEEE Mag. Antennas Propag.*, 50(6):89–98, Dec. 2008.

[44] A. Arboleya, J. Laviada, Y. Álvarez, and F. Las-Heras. Versatile measurement system for imaging setups prototyping. In *2015 9th European Conf. Antennas Propag. (EuCAP)*, pages 1–5, Lisbon, Portugal, Apr. 2015.

[45] A. Tamminen, J. Ala-Laurinaho, and A.V. Räisänen. Indirect holographic imaging at 310 GHz. In *2008 European Radar Conf. (EuRAD)*, pages 168–171, Amsterdam, The Netherlands, Oct. 2008.

[46] G. Junkin. Planar near-field phase retrieval using GPUs for accurate THz far-field prediction. *IEEE Trans. Antennas Propag.*, 61(4):1763–1776, Apr. 2013.

[47] A. Enayati, A. Tamminen, J. Ala-Laurinaho, A.V. RÃ¤isÃ¤nen, G.A.E. Vandenbosch, and W. De Raedt. THz holographic imaging: A spatial-domain technique for phase retrieval and image reconstruction. In *2012 IEEE MTT-S Int. Microw. Symp. Digest (MTT)*, pages 1–3, Montreal, Canada, Jun. 2012.

[48] J. Young, D. Svoboda, and W.D. Burnside. A comparison of time- and frequency-domain measurement techniques in antenna theory. *IEEE Trans. Antennas Propag.*, 21(4):581–583, Jul. 1973.

[49] Y. Huang, K. Chan, and B. Cheeseman. Review of broadband antenna measurements. In *2006 1st European Conf. on Antennas and Propag. (EuCAP)*, pages 1–4, Nice, France, Nov. 2006.

[50] O. Bucci, C. Gennarelli, and C. Savarese. Fast and accurate near-field far-field transformation by sampling interpolation of plane polar measurements. *IEEE Trans. Antennas Propag.*, 39:48–55, Jan. 1991.

IntechOpen